The Journal of the Korean Society of Oceanography
Vol. 32, No. 4, pp. 181-190, December 1997

Bedform Distribution and Sand Transport Trend on a Subtidal Sand Ridge in a Macrotidal Bay, West Coast of Korea

SOO CHUL PARK AND DONG GEUN YOO*
Department of Oceanography, Chungnam National University, Taejon 305-764, Korea
**Korea Institute of Geology, Mining and Materials, Taejon 305-350, Korea*

A large subtidal sand ridge (Jungang Satoe) in Asan Bay, on the west coast of Korea, was studied in order to understand the morphology and sediment transport trend in a macrotidal setting, by means of analyzing sediment samples, current data, side-scan sonographs and seismic profiles. The ridge is about 15 km long and 2-5 km wide, with a relief of about 15 m. It is elongated in the flow direction of flood (SE) and ebb (NW) tidal currents, but asymmetrical in cross section. The western and southwestern side of the ridge is characterized by relatively gentle slopes averaging 0.4°, whereas on the northeastern side, relatively steep slopes were mapped with 1.6° slope angles. Tidal currents associated with the ridge are very strong; maximum surface velocities range from neap values of 50 cm/s to spring values of 130 cm/s. The shear velocities during flood and ebb are strong enough to erode and transport sands on the ridge. Sand waves and megaripples (dunes) are the most common bedforms produced by the tidal currents, which show regional differences in shape and size on the ridge. The distribution pattern of these bedforms indicates that the flood tidal currents are dominant on the offshore (northwest) side of the ridge, whereas the onshore (southeast) side of the ridge is ebb-dominated. The sand transport path as inferred from bedform orientations is directed toward the ridge crest on the flanks, whereas on the crest, it is near-longitudinal to the ridge axis. The convergent, upslope movement of sands on the ridge flanks appears to be important in sand ridge building and maintenance. A significant ridge migration toward the northeast can be suspected on the basis of the ridge morphology, which may cause offshore hazards for navigation.

INTRODUCTION

Tidal sand ridges have been described for numerous places in the world ocean including parts of the North Sea (Stride, 1982; Davis and Balson, 1992), the Yellow Sea (Klein *et al.*, 1982; Zhenxia *et al.*, 1989; Park and Lee, 1994), the East China Sea (Yang and Sun, 1988; Yang, 1989) and the southwest Florida inner shelf (Davis *et al.*, 1993). These ridges are regarded as either active or moribund, depending on their morphology, bedforms, and tidal currents. Study of these sand ridges is important not only for navigation purposes but also for understanding their signature in the stratigraphic record. The changing position of sand ridges usually causes hazards for navigation. Studying the processes and products of modern tidal sedimentation would also provide information to interpret ancient analogues which are widespread in the ancient seas (Davis *et al.*, 1993).

The western coast of Korea in the Yellow Sea has a macrotidal environment with the tidal range up to 9 m and strong tidal currents. Sedimentation by strong tidal currents produce a number of linear sand ridges, which are readily recognized from the topographic maps (Off, 1963; Klein *et al.*, 1982; Korea Institute of Energy and Resources, 1989; Choi and Park, 1992; Choi *et al.*, 1992; Park and Lee, 1994). These tidal sand ridges form bathymetric highs in water depths less than 30-40 m and usually have a length of several tens of kilometres and a relief of more than 10 m above the adjacent sea floor. They are mainly oriented parallel to, or at a small angle with the dominant tidal currents and are regarded as active tidal sand ridges, responding continuously to the present tidal-current system.

We surveyed one large, subtidal sand ridge, Jungang Satoe ('Satoe' means sand body), in Asan Bay, one of the largest, macrotidal bays in the western coast of Korea bordering the Yellow Sea. Most sand ridges on the western coast of Korea develop in the nearshore area (Off, 1963; Klein *et*

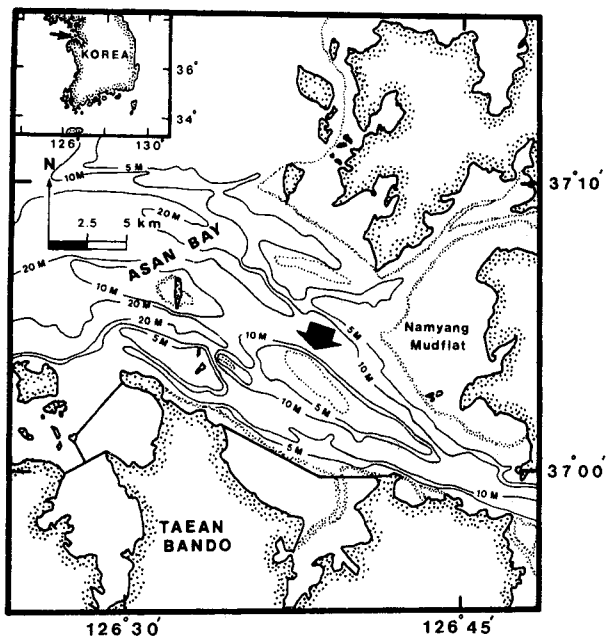

Fig. 1. Index map showing the location of Jungang Satoe (arrow), a subtidal sand ridge in Asan Bay, west coast of Korea. Bathymetry represents the water depth below the lowest low water which is about 4 m below mean sea level. The dotted lines are an area exposed during the lowest low water. Solid lines bordering the Taean Bando show recent dikes for reclamation and freshwater storage.

al., 1982; Park and Lee, 1994), while Jungang Satoe occurs inside the bay. The ridge is oriented NW-SE with a relief of about 15 m above the sea floor (Fig. 1). Asan Bay is an important seaway through which large ships approach the industrial sites on land. Several tidal inlets in the southern and eastern part of Asan Bay have been recently (during the last 15 years) diked and dammed for reclamation and freshwater storage, causing a remarkable decrease of tidal-current speed adjacent to the dikes bordering the Taean Bando (Fig. 1) and the inner part of the bay (Korea Ocean Research and Development Institute, 1994). However, the changes of the tidal current pattern in the main tidal channels and their effect on sedimentation in the bay have not been well studied until now. Thus, it is very important to understand the morphodynamic behaviour of the ridge in response to the present tidal condition, because the changing position of the ridge may cause offshore hazards for navigation. This work was initiated to characterize the nature of this linear sand body, and to understand the morphology and sand transport trend in response to the present tidal-current system, by analyzing the ridge morphology, bedforms, tidal-current data, and sediment samples.

STUDY AREA

Asan Bay is a shallow, coastal embayment in the Ria-type western coast of the Korean Peninsula (Fig. 1). The bay is connected to the Yellow Sea through the northwestern tidal channel which is as deep as 20 m below the lowest low water. The tide in Asan Bay is semidiurnal, with a range of 351 cm during neap tide and 795 cm during spring tide at the entrance of the bay (Korea Maritime and Port Administration, 1991). The mean tidal range is 573 cm. Surface tidal currents flow generally SE during flood and NW during ebb, with the maximum velocity of up to 130 cm/s (Korea Hydrographic Office, 1983). The tidal current velocity decreases considerably toward the inner (eastern) part of the bay. The large tidal range and strong tidal currents in this area produce a complex and dynamic hydraulic regime in terms of sediment erosion and transport (Song *et al.*, 1983; Korea Ocean Research and Development Institute, 1982; Adams *et al.*, 1990).

Jungang Satoe lies in the central part of Asan Bay, surrounded by tidal channels. Fig. 1 shows the location of Jungang Satoe and the bathymetry of the adjacent sea floor which is compiled from the bathymetry chart. The bathymetry represents the water depth below the lowest low water which is about 4 m below mean sea level (Korea Maritime and Port Administration, 1991).

Sediments outside the bay consist largely of well-sorted sands (2-3 ϕ) which have been actively reworked during the postglacial sea-level rise (Korea Ocean Research and Development Institute, 1982). In contrast, the inner part of the bay and intertidal flats are dominated by modern muddy sediments supplied from the Korean rivers. These fine-grained sediments are seasonally resuspended by wave action and transported offshore. The northwesterly wind in winter is considered to be one of the major driving forces for water circulation and dispersal of these fine-grained sediments (Wells, 1988). The northern part of the bay is characterized by the wide mudflat (Namyang Mudflat), with up to 20 m of unconsolidated fine sediment overlying the bedrock. Alexander *et al.* (1991) reported that sediment accumulation rate in this mudflat is 2-9 mm/yr and that the intertidal flat has been actively accreting and prograding seaward. Sea-level data around the Korean Peninsula indicate that sea level approached its present level approximately 5000 yrs B.P. (Bloom and Park, 1985). Most mudflats along the

Yellow Sea coast of Korea are inferred to have been developed since that time (Kim, 1988; Kim and Park, 1992). The adjacent land geology consists mainly of Precambrian metamorphic rocks such as schist, gneiss and quartzite which are intruded by Jurassic granite (Korea Institute of Energy and Resources, 1981). These rocks extend seaward and form the basement rock in Asan Bay.

MATERIALS AND METHODS

The sand ridge (Jungang Satoe) in Asan Bay was extensively studied using a small boat during spring tide. An echosounder (Raytheon model DE-719B) was employed for ridge morphology and detailed bathymetry, while large bedforms on the sand ridge were studied using a side scan sonar system (Klein model 521) that operated at a frequency of 200 kHz and scanned 50 m of both sides of the ship's track. The data were obtained along a 138-km grid of tracklines within the study area (Fig. 2). The ship's speed during the survey was typically 9 km/h. Positioning was maintained with a combination of Radar and Global Positioning System. The sonographs were used to define the wavelengths and orientations of large bedforms (sand waves and megaripples), while the echo-profiles were used to determine their heights and asymmetry. The sonographs were corrected for slant range distortion to determine the true orientation of the bedforms. The Uniboom profiles, previously collected by the National Geographic Institute of Korea, were also examined in order to interpret the geometry and subbottom structure of the ridge. Tidal current data, measured at two stations around the ridge (Korea Maritime and Port Administration, 1991), were available and analyzed to understand the local hydraulic conditions.

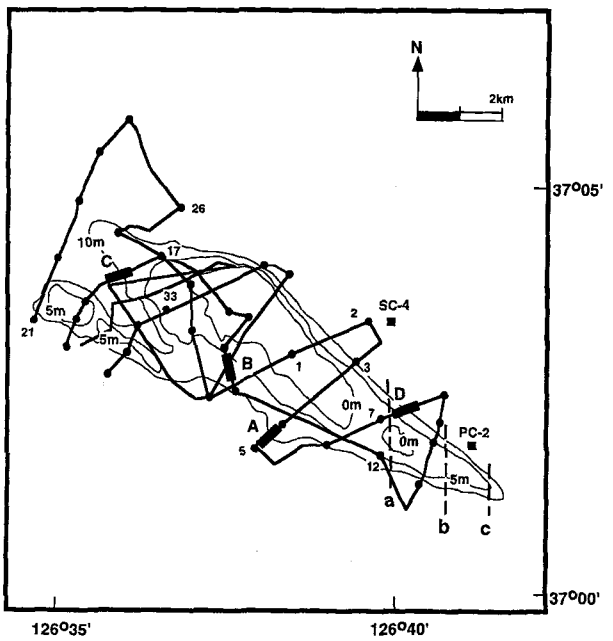

Fig. 2. Map showing the ridge with tracklines of side-scan sonar and echo-sounding survey, and sampling stations of surface sediments (small dots). PC-2 and SC-4 show stations of current measurement (Korea Maritime and Port Administration, 1991), while small dots with numbers are selected sediment samples for analyses of mineralogy and roundness as described in Table 1. Broken lines (a, b, and c) are Uniboom profiles shown in Fig. 3. Heavy lines (A to D) are locations of representative sonographs and echo-sounding profiles of various bedform types shown in Fig. 7.

Along with the bathymetry and side-scan sonar survey, 36 surface sediments were also collected with a Dietz-Lafond grab sampler to determine the grain-size variability and mineralogy. Textural information was also provided by changes in shading on the sonographic records that were caused by differences in grain size. Grain size of sediment samples was determined using a standard dry sieving technique. Sediment statistics were calculated by the method of moments (Griffith, 1967). Ten sediment samples were selected for analyses of mineral composition and roundness measurements of sands. Analyses were conducted on subsamples of the 250-500 μm (2-1 ϕ) fraction; about 300 grains were prepared and counted using a microscope.

RESULTS

Ridge morphology and structure

Jungang Satoe is a linear sand ridge that is asymmetric in cross-section. It extends in a NW-SE direction, which coincides nearly with the flow directions of the prevailing tidal currents. The ridge is about 15 km long and 2-5 km wide, with a relief of about 15 m above the adjacent sea floor. The profiles across the ridge along the tracklines show that sand-ridge slopes are asymmetric in cross section; the western and southwestern side of the ridge is characterized by relatively gentle slopes averaging 0.4°, whereas on the northeastern side of the ridge, relatively steep slopes were mapped with 1.6° slope angles (Fig. 2). The crest zone of the ridge is relatively flat compared to the ridge flanks.

Fig. 3 shows the Uniboom records in the sou-

theastern side of the ridge in N-S directions. The Uniboom profiling was conducted over several hundreds of kilometres in Asan Bay as a coastal mapping project by the National Geography Institute of Korea. The profiles show the asymmetric geometry of the ridge, with the flat crest zone. There is little indication of stratification within the ridge except a few subtle reflectors detected in the trough region (Fig. 3b). This transparent aspect of the ridge is presumably due to the homogeneous nature of the sand, both in grain size and mineralogy (Davis and Balson, 1992). Generally, the lower boundary of the ridge sequence is not easily identified on the Uniboom records, because of the limit of acoustic penetration into the thick sand layer. However, based on the small-scale impedance contrast of an indistinct reflector in the trough region, the maximum thickness of sand ridge is estimated about 15 m.

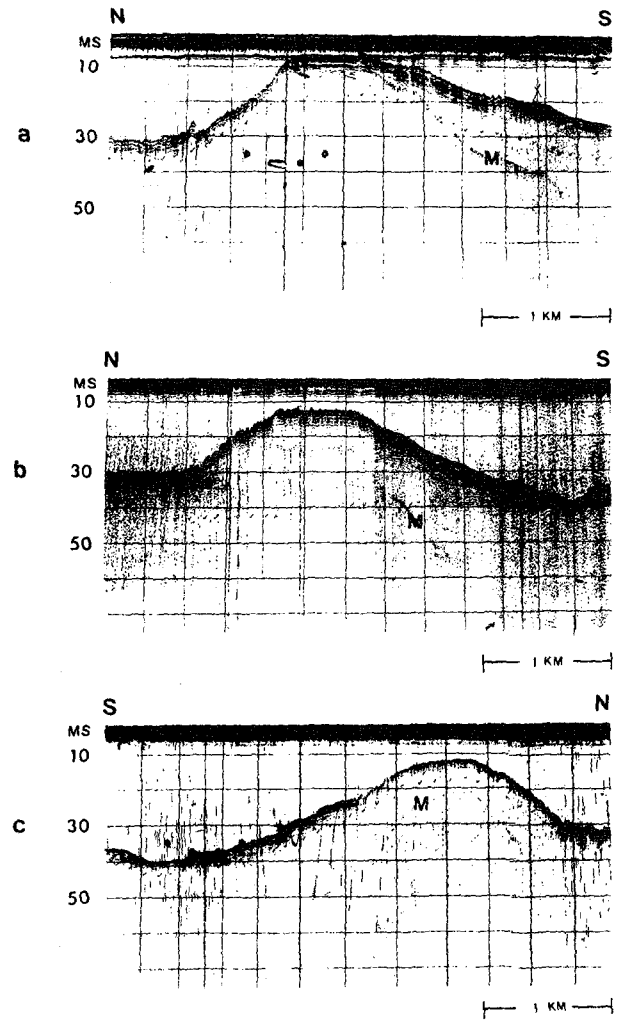

Fig. 3. Uniboom profiles across the ridge in a N-S direction, showing the asymmetric geometry and subsurface structure (M; multiple) (for location, see Fig. 2). Vertical axis is two-way time (milliseconds) and 10 ms corresponds to approximately 8 m of sediment thickness.

Sediment texture and mineralogy

Data on surface sediments obtained from Jungang Satoe show the sediments on the ridge consist of poorly to well-sorted sand with a mean grain size between -1 ϕ and 4 ϕ (Fig. 4). The coarse sand with a mean grain between -1 ϕ and 1 ϕ is dominant on the northwestern part of the ridge, while the sediments on the southeastern part consist mainly of medium sand with a mean size between 1 ϕ and 2 ϕ. The sediments on the middle part of the ridge surface consist of fine to very fine sand with a mean size of 3-4 ϕ. This pattern of grain-size variability appears to be closely related with the distribution pattern of bedform types; those areas dominated by sand waves and megaripples are generally floored by coarse to medium sand, while fine to very fine sand is associated with the flat bedform type (Fig. 8). The sorting values show much variability on the ridge surface, ranging from 0.5 ϕ to 3 ϕ, although the sediments show a general trend of better sorting on the ridge crest. The sediments on the northwestern and southeastern flanks of the ridge surface are relatively better sorted than those on the northeastern and southwestern flanks (Fig. 4). In contrast to the ridge surface, the adjacent sea floor including the southwestern and northeastern trough region of the ridge is floored by poorly to very poorly sorted (> 1.5 ϕ) silty sand.

Mineralogical analyses completed on the medium sand-size fraction (1-2 ϕ) of selected sediment samples from the ridge crest and flanks reveal that the sands are subarkose or sublithic arenite in composition (nomenclature after Pettijohn, 1975), consisting mainly of quartz (55-90%), feldspar (8-22%), and rock fragments (2-23%) (Table 1). Heavy minerals occur in small but undetermined amounts through the samples. These sands appear to have been ultimately derived from crystalline rocks exposed on the adjacent land. Roundness measurements show that the sands are subangular (2.95-3.40, after Powers; 1953), indicative of low maturity. These roundness values are very similar to those found on other sand ridges in the eastern Yellow Sea (Klein et al., 1982; Park and Lee, 1994). The sands in the study area may represent an early stage of tidal abrasion.

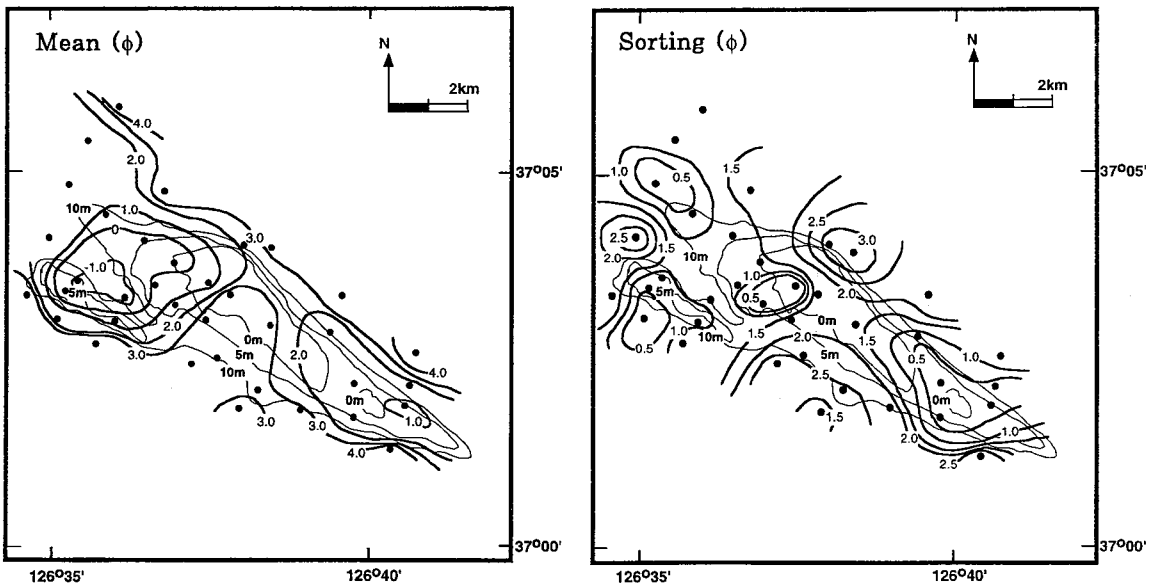

Fig. 4. Distribution of mean and sorting values of surface sediments on the ridge in ϕ unit.

Table 1. Mineral composition, roundness (after Powers, 1953), and texture of selected sediment samples collected from Juangang Satoe in the Yellow Sea coast (for sample station, see Fig. 2). Mineral composition and roundness values represent the medium sand fraction (250-500 μm). Q: quartz, F: feldspar, RF: rock fragment

Station	Mineral Composition (%)			Roundness	Mean	Sorting
	Q	F	RF		(ϕ)	(ϕ)
1	61.06	22.18	16.76	2.95	3.42	1.51
2	89.62	9.56	0.90	3.10	3.77	2.36
3	80.06	10.11	9.83	3.20	1.47	0.52
5	77.56	8.25	14.19	3.40	2.82	1.12
7	66.88	12.54	20.58	3.15	1.53	0.56
12	79.41	8.56	12.03	3.00	1.23	0.40
17	87.82	8.67	3.51	3.00	0.80	1.16
21	88.53	9.74	1.73	3.20	3.80	1.92
26	77.80	16.96	7.13	3.30	3.93	1.73
33	84.38	8.93	6.69	3.30	0.53	1.23
Average	72.72	15.56	11.73	3.13	1.98	1.37

Tidal current data

Tidal currents were measured at two stations (PC-2 and SC-4, Fig. 2). Station PC-2 is located on the northern flank of the southeastern end of the ridge, while station SC-4 is located in the northern trough at the center of the ridge. The mean water depth is 14 m and 16 m, respectively. At station PC-2, measurements were made continuously at 10 minutes interval for a two-week period during October, 1991. An Aanderaa RCM-4 type current meter was moored in the mid-depth (7 m below the sea surface) over the entire period. Both spring and neap tidal conditions were included. Tidal current data from this station are displayed in time-velocity curves for 24 hours representing spring, mean, and neap tide (Fig. 5). Tidal direction data over the entire period were described as a rose diagram of 16 directions (Fig. 6).

Time-velocity curves (Fig. 5) typically show nearly symmetric patterns with little or no semi-diurnal inequality, although there is semidiurnal inequality depending on the lunar cycle in this area. Maximum current velocities range from neap values of 50 cm/s to spring values of 130 cm/s. During each tidal cycle in spring and mean tide, current velocities of more than 50 cm/s are maintained for several hours. For the fine to medium sands, the surface current velocity of about 50 cm/s has been suggested as the level above which a significant sediment transport takes place and large bedforms become well-developed (Kenyon *et al.*, 1981; Stride, 1982). The peak tidal currents occur generally about 3 hours before high and low tide. The sea level and current obser-

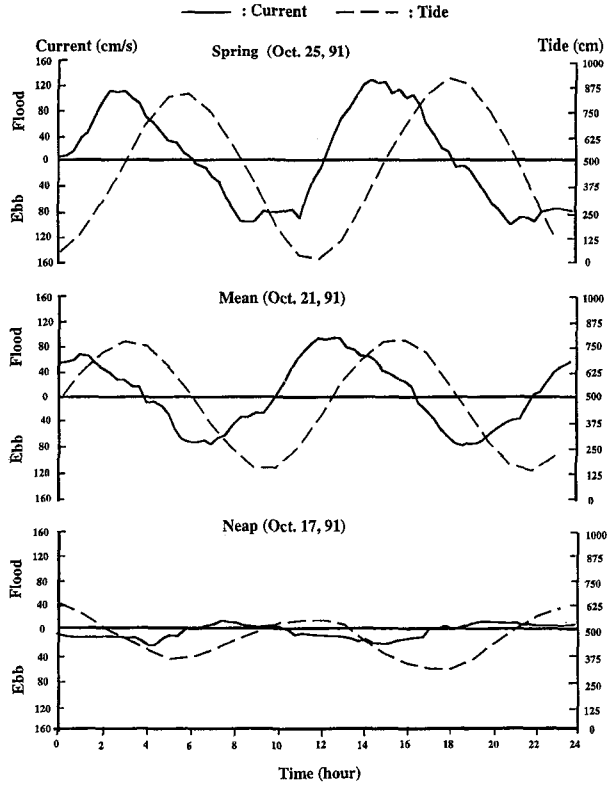

Fig. 5. Time-velocity curves showing variations of speed (solid line) and tide (broken line) during spring, mean, and neap tide, measured at station PC-2 (for location, see Fig. 2).

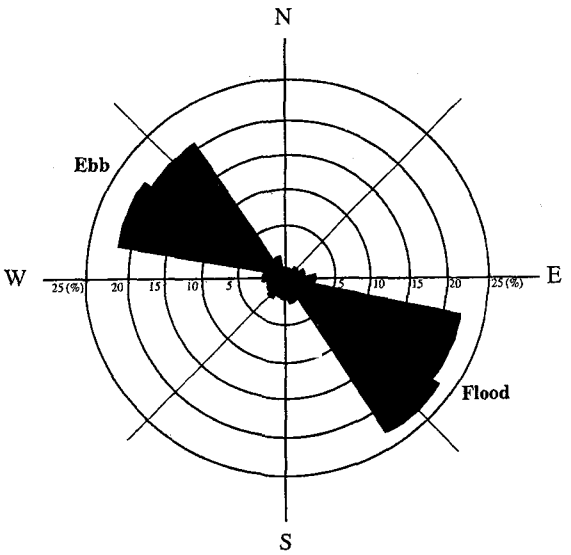

Fig. 6. A rose diagram showing directions of the dominant tidal currents during flood and ebb, measured for 14 days at station PC-2 (No. of data=2016).

ved at PC-2 suggest that the tide in this area is a standing-wave type. The current rose diagram (Fig. 6) indicates that the dominant flow direction of tidal currents is SE or ESE during flood and NW or WNW during ebb. Tidal current data from station PC-2 show patterns quite reminiscent of those measured on a large tidal sand ridge in the nearshore along the Yellow Sea coast (Park and Lee, 1994).

Table 2. Tidal current velocity in surface (3.3 m depth), mid-depth (9.6 m depth), and near-bottm (3 m above the sea bed), measured at station SC-4 during spring tide for one tidal cycle (12.5 hours). The positive values represent flood currents flowing SE and the negative ones are ebb currents flowing NW. The bottom shear velocities (U*), estimated from the near-bottom velocities, are also shown

Station: SC-4 Depth: 16 m Spring Tide				
Oct. 22, 1991	Surface	Mid-depth	Bottom	Shear Velocity
Time	U (cm/s)	U (cm/s)	U (cm/s)	U* (cm/s)
6:30	-84	-70	-55	3.44
7:00	-90	-82	-68	4.25
8:00	-89	-78	-55	3.44
9:00	-67	-60	-31	1.94
10:00	-30	-25	-12	0.75
11:00	+29	+28	+16	1.00
12:00	+80	+70	+59	3.69
13:00	+96	+80	+70	4.38
14:00	+91	+78	+55	3.44
15:00	+73	+65	+36	2.25
16:00	+38	+33	+20	1.25
17:00	-25	-23	-18	1.13
18:00	-67	-59	-41	2.56
19:00	-93	-85	-68	4.25
Average	68	60	43	2.70

Table 2 includes the tidal current data measured at station SC-4. The data were collected in the surface (3.2 m below the sea surface), mid-depth (9.6 m below the surface), and bottom layer (3 m above the sea bed) for one tidal cycle (12.5 hours) during spring tide. The mean current velocities at these depths are 68 cm/s, 60 cm/s, and 43 cm/s, respectively. The current velocity decreases slightly from the surface to near the bottom; however, there is little deviation of current directions with depth. The near-bottom current velocities were analyzed for an estimation of the boundary shear velocity at the sea bed, assuming that the vertical velocity distribution in the bottom boundary layer is logarithmic (Middleton and Southard, 1984; Dyer, 1986). The vertical velocity profile in this turbulent boundary layer can be generally expressed by the von Karman-Prandtl equation

$$\frac{U}{U^*} = \frac{1}{\kappa} \ln \frac{y}{y_o}$$

where U is the mean current velocity at a distance y above the sea bed; U* is the shear velocity; κ is von Karman's constant (approximately 0.4); y_o is the roughness height. It has been proven by nume-

rous researchers that this equation can fairly approximate the velocity distribution in the bottom boundary layer of wide open channels (Sternberg, 1968, 1972; Smith and McLean, 1977; Choi, 1991). The shear velocities calculated by this equation are also presented in Table 2. The roughness height in this area is assumed to be 0.5 cm as suggested by Choi (1991). The shear velocities range from 0. 75 to 4.38 cm/s, with a mean value of 2.70 cm/s. The shear velocities during flood and ebb are usually much higher than the critical shear velocity which is experimentally estimated to be about 1.4 cm/s for fine to medium sand (Miller *et al.*, 1977; Self *et al.*, 1989; Choi, 1991). However, the shear velocities associated with turning of tide are lower than the critical value. The data suggest that the sandy sediment that typifies the sand ridge can be moved by tidal currents for several hours during each tidal cycle.

Bedform types

Side-scan sonographs and echo-sounding profiles reveal a series of large-scale bedforms on the ridge; sand waves and megaripples (dunes) are the most common bedforms, which have been used as a good indicator of the net sediment transport. Megaripples occur independently or are superimposed on sand waves. Bedforms associated with Jungang Satoe show regional differences in shape and size, and can be classified into 4 types. Fig. 7 represents side-scan records and echo-profiles of each type. The distribution of bedform types is shown in Fig. 8.

Bedform type A is characterized by a flat bed; sonograph and echo-profile (Fig. 7-A) show a featureless ground. This type of bedform was found primarily on the lower flanks and troughs of the ridge where water depth is deeper than about 10 m, and partly on the crest area. Bedform type B (Fig. 7-B) consists of megaripples (dunes) which have a wavelength of 5-10 m and a height of 30-50 cm. The wavelength/height ratio is generally between 10 and 30. Megaripples are present primarily on the crest, and are less common on the flank of the ridge. Bedform type C (Fig. 7-C) is large sand waves with a wavelength of 60-100 m and a height of 2-3 m. The wavelength/height ratio is between 30 and 50. Sand waves on the flanks of the ridge are asymmetric in cross section with steeper slip faces oriented in the upslope direction. Typically, their crestlines are straight. This type of sand waves is found over a broad area of the western and northern slope of the ridge. Bedform type D (Fig. 7-D) represents sand waves that show deformed, rounded-off features. This type of sand waves occurs mainly

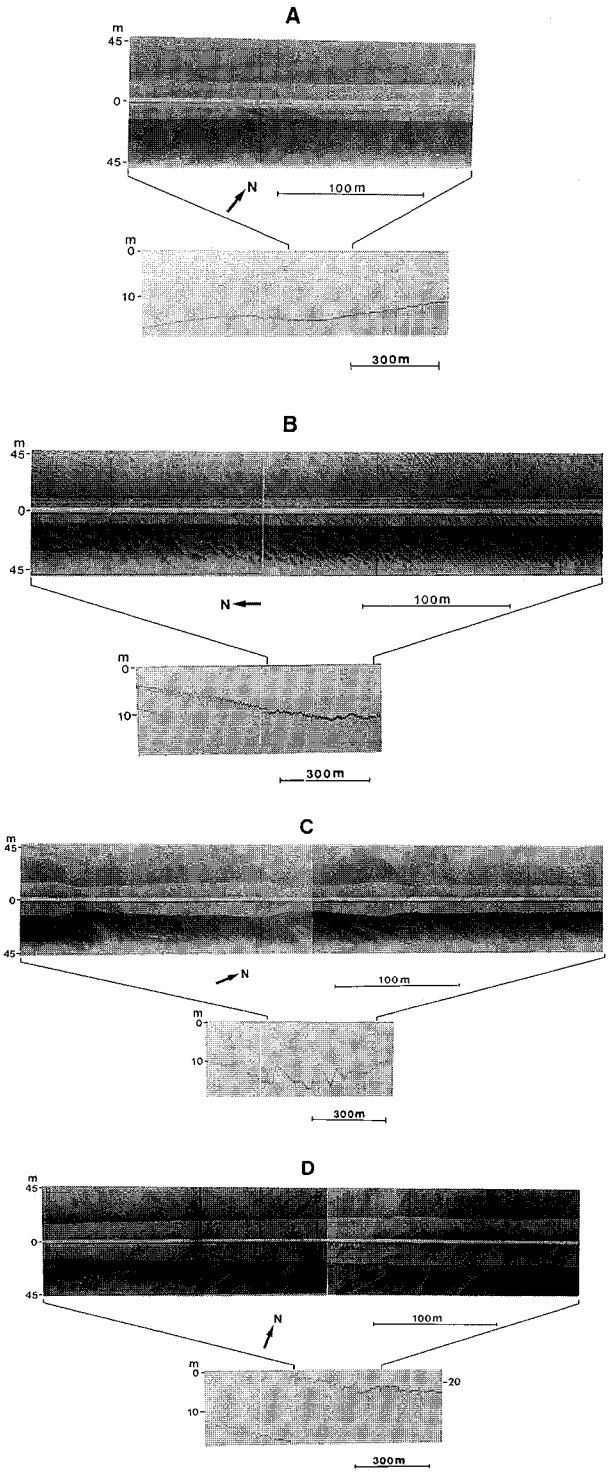

Fig. 7. Sonographs and echo-sounding profiles showing bedform types A, B, C, and D, respectively, which have been mapped in Fig. 8 (for location, see Fig. 2). See text for explanation of bedform types.

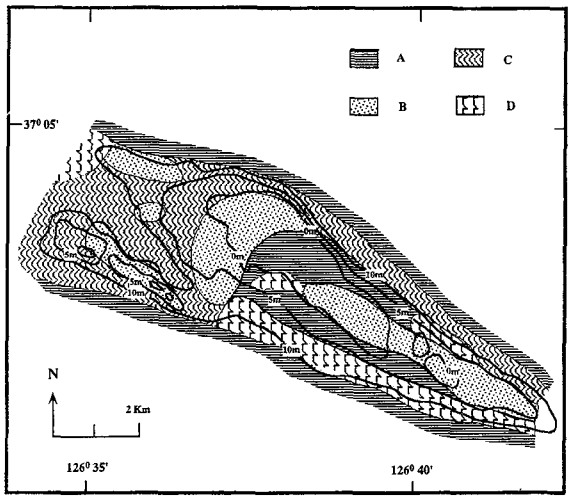

Fig. 8. Distribution of bedform types shown in Fig. 7. A: flat bed, B: megaripple (dune), C: sand wave, D: deformed sand wave.

on the southeastern slope of the ridge and at a few locations in other parts of the ridge. They are irregular in morphology, with a wavelength of 20-30 m and a height usually less than 1 m.

Sand waves are present on both the steep and gentle slopes of the ridge. They are aligned about 60-90° to the strike of the ridge axis. Those on the gentle, northwestern slope are oriented mainly northeast-southwest, while on the steep northeastern slope they trend north-south. Sand waves on the gentle, southern slope are oriented mainly east-west. Generally, the profile of sand waves on both the gentle and steep slopes is asymmetric, with their slip-faces apparently toward the ridge crest. The echo-sounding and side-scan sonar survey was started from the western part of the sand ridge at the beginning of flood, and was ended at nearly the same site at the end of ebb tide. During the survey, the steeper sides of sand waves on the flanks of the ridge faced toward the ridge crest regardless of the turning of the tide. The good preservation of these bedforms indicates that they are relatively stable. However, many sand waves (type D) in the southern slope with irregular and rounded-off crests indicate some modification in response to the turning of tidal currents.

Typically, the megaripples are present on or near the crest of the ridge and, with few exceptions, have a northeast-southwest orientation. Megaripples are also present on the flanks of the ridge, where they are superimposed on the sand waves. The crestlines of megaripples are generally normal to the strike of the ridge axis, although their asymmetry could not be determined by our seismic systems.

DISCUSSION

Sediment transport is evident in those areas where large bedforms (sand waves and megaripples) were found. In these areas, bedload transport of sand is assumed to be perpendicular to the crestlines of bedforms, and the direction of sediment transport is indicated by bedform asymmetry. Fig. 9 shows the direction of sand transport on the basis of sand-wave asymmetry and orientation of megaripples. In the northwestern gentle slope of the ridge where the asymmetry of sand waves could be determined, the net bottom transport direction was found to be dominantly toward southeast, whereas it shows a trend toward west in the northeastern steep slope. In the southern slope of the ridge, the net transport was determined to be toward north or northwest. This transport pattern indicates that the northwestern side of the ridge is mainly influenced by flood tidal currents, while on the northeastern and southern side, ebb tidal current is dominant. The transport pattern of sands on the ridge crest is assumed to be nearly parallel to the ridge axis, although the directional data could not be resolved by our side-scan sonar and echo-sounding records because of difficulty in determining the direction of asymmetry of the megaripples. The convergent, upslope movement of

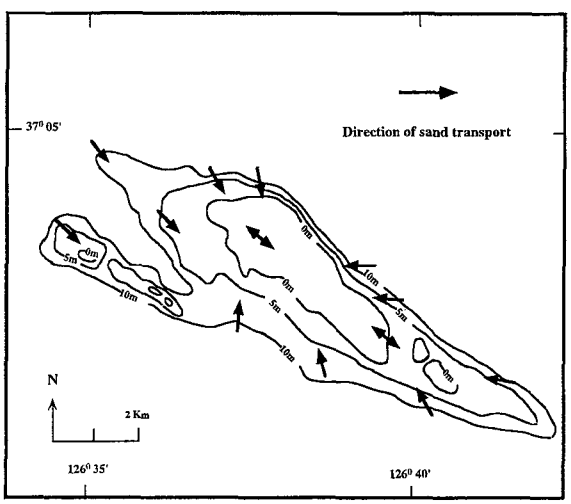

Fig. 9. The directions of sand transport on the ridge flanks and crest as inferred from sand wave asymmetry and megaripple (dune) orientations. The bedload transport of sands on the flanks are directed upslope toward the ridge crest with an angle of up to 60° relative to the dominant tidal currents, while it is near-longitudinal to the ridge-axis on the crest.

sands on the ridge flanks seems to be important in sand ridge building and maintenance.

Previous study of a tidal sand body in the southeastern Yellow Sea (Klein *et al.*, 1982) reported that the ridge flanks are dominated by near-longitudinal sand dispersal, whereas the ridge crest is dominated by cross-ridge dispersal. They proposed a trapezoidal sand dispersal model and suggested that there is a major component of flow at right angles to the sand-body axis prior to or during the turning of tide. This flow was observed at 0.5 m above the sea bed and is considered to be responsible for cross-ridge sand transport on the crest. However, we could not confirm such a mode of transport on Jungang Satoe. The transport trend of sands on Jungang Satoe, as determined from bedform orientations, is aligned apparently toward the ridge crest on the ridge flanks, whereas it is near-longitudinal on the ridge crest. A possible explanation for this difference is that Jungang Satoe is now in a state of disequilibrium with the present-day tidal currents. The changed tidal current system after recent construction of dams and dikes in Asan Bay has presumably been reshaping and modifying the ridge geometry. The asymmetric morphology of the ridge, with the northeastern slope steeper than the western and southern slope, indicates a net migration direction of the ridge toward northeast, although we did not observe any inclined bedding parallel to the steeper ridge slope on the seismic profiles. A comparison of the 1985 and 1993 bathymetric charts (Park, 1994) shows that the ridge has migrated about 500 m toward northeast during this period. This migration of the ridge toward northeast could cause offshore hazards for navigation, because most large ships approach the land through the northern channel of the ridge.

Tidal sand ridges in the nearshore area of the west coast of Korea are supposed to be late Holocene features (Klein *et al.*, 1982; Korea Institute of Energy and Resources, 1989; Choi and Park, 1992; Park and Lee, 1994), and not a relict feature representing a different depositional regime associated with a lower stand of sea level followed by subsequent transgression. Mineralogical and sediment texture data suggest that a majority of sands forming Jungang Satoe represents an early stage of tidal abrasion and is mainly derived from the coastal erosion by strong tidal currents. The river-origin of sand could be neglected as the drainage systems in Asan Bay are extremely limited. The seismically transparent aspect of the ridge sequence appears to be due to the homogeneous nature of the sediment. A similar active tidal sand ridge has been also reported from the nearby Gyeonggi Bay (Korea Institute of Energy and Resources, 1989); the lowermost part of the ridge sequence is dated approximately 3000-5000 yrs BP. Although we did not recover any material that is dateable to determine the exact age of deposition, we suspect that the depositional age for Jungang Satoe is similar to that of the Gyeonggi Bay tidal sand ridge. Further research is required for the stratigraphic interpretation of the ridge sequence to understand the genesis and evolutionary pattern of Jungang Satoe in the late Holocene time.

CONCLUSIONS

Data from analyses of a subtidal sand ridge (Jungang Satoe) in Asan Bay permit some general conclusions which probably characterize other active sand ridges along the Yellow Sea coast of Korea.

1) Jungang Satoe is an active subtidal sand ridge which is asymmetrical in cross-section and linear in plan. The surface of the ridge is composed of sand with a mean grain size between 0.5 ϕ and 4 ϕ. Mineralogically, the sand is a subarkose or a sublithic arenite, consisting mainly of quartz (55-90%), feldspar (8-22%), and rock fragments (2-23%). Seismic records show a transparent aspect of the ridge sequence, indicative of the homogeneous nature of both the grain size and mineralogy.

2) Tidal current data associated with Jungang Satoe show nearly symmetrical patterns with little semi-diurnal inequality during flood and ebb. Maximum surface velocities range from neap values of 50 cm/s to spring values of 130 cm/s. The calculated shear velocities at the sea bed indicate that a significant sand transport takes place on the ridge for several hours of each tidal cycle during spring and mean tide.

3) A variety of bedforms of different size occurs on the sand ridge; large sand waves are most common on the ridge flanks, whereas on the crest, megaripples (dunes) are dominant. The asymmetrical patterns of sand waves on the ridge flanks, with their slip-faces apparently toward the ridge crest, indicate the consistent, upslope flow components of tidal currents which are important in sand ridge building and maintenance. However, the sand transport trend on the crest appears to be near-

longitudinal, parallel to the dominant tidal currents.

4) The ridge represents the late-Holocene feature, and the migration pattern may cause offshore hazards for navigation in the bay.

ACKNOWLEDGMENTS

This study was supported by the Academic Research Fund of Ministry of Education, Republic of Korea (KIOS-97-M-16). We express our appreciation to the National Geographic Institute of Korea for providing the unpublished Uniboom data. Drs. M.J. Park, D.J.P. Swift and J.H. Choi and one anonymous reviewer gave many helpful suggestions to improve the draft of the text.

REFERENCES

Adams, C.E., J.T. Wells and Y.A. Park, 1990. Internal hydraulics of a sediment-stratified channel flow. *Mar. Geol.*, **95**: 131-145.

Alexander, C.R., C.A. Nittrouer, D.J. DeMaster, Y.A. Park and S.C. Park, 1991. Macrotidal mudflats of the southwestern Korean coast: a model for interpretation of intertidal deposits. *J. Sedim. Petrol.*, **61**: 805-824.

Bloom, A.L. and Y.A. Park, 1985. Holocene sea-level history and tectonic movement, Republic of Korea. *Quat. Res.*, **24**: 77-84.

Choi, D.L., S.R. Kim, B.C. Suk and S.J. Han, 1992. Transport of sandy sediments in the Yellow Sea off Tae-An Peninsula, Korea. *J. Korean Soc. Oceanogr.*, **27**: 66-77.

Choi, J.H., 1991. Estimation of boundary shear velocities from tidal current in the Gyeonggi Bay, Korea. *J. Korean Soc. Oceanogr.*, **26**: 340-349.

Choi, J.H. and Y.A. Park, 1992. Textural characteristics and transport model of surface sediments of a tidal sand ridge in Gyeonggi Bay, Korea. *J. Korean Soc. Oceanogr.*, **27**: 145-153.

Davis, R.A. and P.S. Balson, 1992. Stratigraphy of a North Sea tidal sand ridge. *J. Sedim. Petrol.*, **62**: 116-121.

Davis, R.A., J. Klay and P. Jewell, 1993. Sedimentology and stratigraphy of tidal sand ridges: Southwest Florida inner shelf. *J. Sedim. Petrol.*, **63**: 91-104.

Dyer, K.R., 1986. Coastal and Estuarine Sediment Dynamics. Wiley, New York. 342pp.

Griffith, J.C., 1967. Scientific Method in Analysis of Sediments. McGraw-Hill, New York. 508pp.

Kenyon, N.H., R.H. Belderson, A.H. Stride and M.A. Johnson, 1981. Offshore tidal sand banks as indicators of net sand transport and as potential deposits. In: Holocene Marine Sedimentation in the North Sea Basin, edited by S.D. Nio, R.T.E. Schuttenheim and T.C.E. van Weering, Int. *Assoc. Sedim., Spec. Publ.*, **5**: 257-268.

Kim, Y.S., 1988. Sedimentary environments and evolution of intertidal deposits on Sajangpo Coast, Chonsu Bay, west coast of Korea. Ph.D. thesis, Seoul Natl. Univ., Seoul, Korea, 169pp.

Kim, Y.S. and S.C. Park, 1992. Stratigraphy and evolution of the intertidal deposits in Gunhung Bay, west coast of Korea. *J. Korean Soc. Oceanogr.*, **13**: 41-52.

Klein, G.D., Y.A. Park, J.H. Chang and C.S. Kim, 1982. Sedimentology of a subtidal, tide-dominated sand body in the Yellow Sea, southwest Korea. *Mar. Geol.*, **50**: 221-240.

Korea Hydrographic Office, 1983. Tidal Current Charts (Incheon Hang and Approaches), 26pp.

Korea Institute of Energy and Resources, 1981. Geological Map of Korea.

Korea Institute of Energy and Resources, 1989. Report on the Detailed Investigative Techniques for Exploring Shallow Marine Clastic Mineral Deposits, 216pp.

Korea Maritime and Port Administration, 1991. Report on the Prevention of Channel Sedimentation in Asan Bay, 296pp.

Korea Ocean Research and Development Institute, 1982. Report on Marine Geology of Asan Bay, 186pp.

Korea Ocean Research and Development Institute, 1994. Sedimentary Effects of Break-water Construction on Coastal Environments, 174pp.

Middleton, G.V. and J.B. Southard, 1984. Mechanics of Sediment Movement. *Soc. Econ. Paleont. Miner.*, Short Course, 3.

Miller, M.C., I.H. McCave and P.D. Komar, 1977. Threshold of sediment motion under unidirectional currents. *Sedimentology*, **24**: 507-527.

Off, T., 1963. Rhythmic linear sand bodies caused by tidal currents. *Bull. Am. Ass. Petrol. Geol.*, **47**: 339-341.

Park, S.C., 1994. Recent sedimentary environment in Asan Bay. In: Proceedings of Symposium on Marine Environment of Asan *Bay. Res. Inst. Mar. Sci.*, Chungnam Natl. Univ., Taejon, Korea.

Park, S.C. and S.D. Lee, 1994. Depositional patterns of sand ridges in tide-dominated shallow water environments: Yellow Sea coast and South Sea of Korea. *Mar. Geol.*, **120**: 89-103.

Pettijohn, F.J., 1975. Sedimentary Rocks. Harper Int., New York, 628pp.

Powers, M.C., 1953. A new roundness scale for sedimentary particles. *J. Sedim. Petrol.*, **23**: 117-119.

Self, R.F.L., A.R.M. Nowell and P.A. Jumars, 1989. Factors controlling critical shears for deposition and erosion of individual grains. *Mar. Geol.*, **86**: 181-199.

Smith, J.D. and S.R. McLean, 1977. Spatially averaged flow over a wavy surface. *J. Geophy. Res.*, **82**: 1735-1746.

Song, Y.O., D.H. Yoo and K.R. Dyer, 1983. Sediment distribution, circulation and provenance in a macrotidal bay: Garolim Bay, Korea. *Mar. Geol.*, **52**: 121-140.

Sternberg, R.W., 1968. Friction factors in tidal channels with differing bed roughness. *Mar. Geol.*, **6**: 243-260.

Sternberg, R.W., 1972. Predicting initial motion and bed-load transport of sediment particles in the shallow marine environment. In: Shelf Sediment Transport Process and Pattern, edited by D.J.P. Swift, D.B. Duane and O.H. Pilkey, Hutchinson and Ross, Dowden.

Stride, A.H., 1982. Offshore Tidal Sands, Processes and Deposits. Chapman and Hall, London, 222pp.

Wells, J.T., 1988. Distribution of suspended sediment in the Korea Strait and southeastern Yellow Sea: Onset of winter monsoons. *Mar. Geol.*, **28**: 461-482.

Yang, C.S., 1989. Active, moribund and buried tidal sand ridges in the East China Sea and the Southern Yellow Sea. *Mar. Geol.*, **88**: 97-116.

Yang, C.S. and Sun, J.S., 1988. Tidal sand ridges on the East China Sea shelf. In: Tide-influenced Sedimentary Environments and Facies, edited by P.L. de Boer, A. van Gelder and S.D. Nio, Reidel, Dordrecht.

Zhenxia, L., H. Yichang and Z. Qinian, 1989. Tidal current ridges in the southwestern Yellow Sea. *J. Sedim. Petrol.*, **59**: 432-437.